Available online at www.sciencedirect.com
SCIENCE DIRECT®
Journal of Magnetic Resonance 160 (2003) 47–51
JMR Journal of Magnetic Resonance
www.elsevier.com/locate/jmr

The elimination of magnetic susceptibility artifacts in the micro-image of liquid–solid interfaces: internal gradient modulation by the CPMG RF train

Andrej Duh,[a,*] Aleš Mohorič,[b] Janez Stepišnik,[b,c] and Igor Serša[c]

[a] *Faculty of Electrical Engineering and Computer Science, Institute of Mathematics and Physics, University of Maribor, Smetanova 17, 2000 Maribor, Slovenia*
[b] *Faculty of Mathematics and Physics, Physics Department, University of Ljubljana, Jadranska 19, 1000 Ljubljana, Slovenia*
[c] *Institute Josef Stefan, Jamova 39, 1000 Ljubljana, Slovenia*

Received 3 June 2002; revised 4 October 2002

Abstract

Distortions of magnetic resonance images near solid–liquid interface appear as the result of the restriction to spin self-diffusion in the proximity of impermeable boundary as well as of a susceptibility difference. The spectral analysis of spin echo enables to resolve, in a simple way, how various RF-gradient pulse sequences reduce the effect of the internal magnetic field induced by the susceptibility difference at interfaces. The 1D diffusion-weighted imaging of water in the narrow notch tested efficiency of some sequence. The notch was milled in a piece of Plexiglas. The method can be used to distinguish the susceptibility effect from the effects of applied gradients when investigating the transport of fluid through a porous structure.

Keywords: Spin echo; Magnetic resonance; Gradient; Diffusion-weighted imaging; Edge enhancement; Susceptibility difference; Porous media

1. Introduction

Magnetic resonance imaging (MRI) relies on the application of magnetic field gradients to encode spatial information in the precession frequency of local spins. The contrast of an extreme spatial resolution MR micro-image tends to be diffusion weighted. Edge enhancement near a solid–liquid interface appears as the result of restricted diffusive motion in the proximity of impermeable walls [1–3]. In the high magnetic field, the non-uniform magnetic field, caused by the susceptibility difference at the solid–fluid interface, affects the signal in the same way as a steady external magnetic field gradient [4–7]. Therefore, micro-imaging artifacts at interfaces come from the restriction to motion as well as from the attenuation induced by internal susceptibility magnetic field gradient $\mathbf{G}_s(\mathbf{r})$. This gradient can be treated as a contribution to the applied magnetic field gradient $\mathbf{G}_a$ yielding the total magnetic field gradient [8]

$$\mathbf{G}(\mathbf{r}) = \mathbf{G}_a + \mathbf{G}_s(\mathbf{r}). \tag{1}$$

At the echo time τ, spin motion through a non-uniform magnetic field perturbs the phase of an individual spin by $\theta(\tau) = \gamma \int_0^\tau \mathbf{G}(t)\cdot\mathbf{r}(t)\,dt = -\int_0^\tau \mathbf{F}(t)\cdot\mathbf{v}(t)\,dt$, where $\mathbf{F}(t) = \gamma\int_0^t \mathbf{G}(t')\,dt'$ is a factor of spin dephasing, $\mathbf{r}(t)$ is the spin displacement and $\mathbf{v}(t)$ is the spin velocity.

For the PGSE sequence of two short gradient pulses, each of duration δ and separated by Δ, $\mathbf{F} = \gamma\delta\mathbf{G}$, the mean of the spin phase random fluctuation can be analyzed with the probability distribution (the diffusion propagator) [8–10]. However, in cases of finite gradient pulses, multi-pulse gradients combined with RF pulses or gradients of a general waveform, the short gradient pulse approximation fails, and stochastic properties of the spin location have to be transformed to the stochastic properties of the spin velocity. In this case, a method of the statistical physics, called the cumulant expansion of the characteristic functional, can be used

* Corresponding author. Fax: +386-2-251-1178.
E-mail address: andrej@fiz.uni-lj.si (A. Duh).

1090-7807/02/$ - see front matter © 2002 Elsevier Science (USA). All rights reserved.
PII: S1090-7807(02)00111-8

to treat the spin phase average [11]. This expansion, truncated in the Gaussian approximation, gives the spin echo as

$$E(\tau) = \int_V E(\mathbf{r}) e^{i\phi(\mathbf{r},\tau)-\beta(\mathbf{r},\tau)}\, d\mathbf{r}, \tag{2}$$

where $E(\mathbf{r})$ is the normalized echo of the spin subensemble at the location $\mathbf{r}$. The phase shift

$$\phi(\mathbf{r},\tau) = -\int_0^\tau \mathbf{F}(\mathbf{r},t)\langle \mathbf{v}(\mathbf{r},t)\rangle\, dt \tag{3}$$

results from the spin scattering on boundaries and depends on the mean local velocity. Its distribution within the pore yields the so-called diffusive diffraction of the total spin echo signal [12], when the wavelength of the phase grating created by the applied gradient $2\pi/F$ equals the mean spin displacement. The spin echo attenuation depends on the local velocity correlation function (VCF)

$$\beta(\mathbf{r},\tau) = \frac{1}{2}\int_0^\tau \int_0^\tau \mathbf{F}(\mathbf{r},t)\cdot\langle \mathbf{v}(\mathbf{r},t)\mathbf{v}(\mathbf{r},t')\rangle_c \cdot \mathbf{F}(\mathbf{r},t')\, dt\, dt'. \tag{4}$$

Micro-imaging of the signal magnitude discards the phase shifts yielding the diffusion-weighted distribution dependent only on the attenuation Eq. (4), though the effect of the phase shift remains in the last term of the effective velocity correlation as

$$\langle \mathbf{v}(\mathbf{r},t)\mathbf{v}(\mathbf{r},t')\rangle_c = \langle \mathbf{v}(\mathbf{r},t)\mathbf{v}(\mathbf{r},t')\rangle - \langle \mathbf{v}(\mathbf{r},t)\rangle\langle \mathbf{v}(\mathbf{r},t')\rangle. \tag{5}$$

In the case of restricted diffusion near an impermeable flat boundary lying in yz plane, the average of transverse velocity component at position x is given by

$$\langle v_x(x,t)\rangle = \sqrt{\frac{D}{\pi t}} e^{-\frac{x^2}{4Dt}} \tag{6}$$

and the velocity correlation function is

$$\langle v_x(x,t)v_x(x,0)\rangle = 2D\delta(t) + \frac{x(2Dt-x^2)}{4\sqrt{\pi D t^5}} e^{-\frac{x^2}{4Dt}}. \tag{7}$$

Clearly, only the diffusive motion of the spins within the distance $\sqrt{Dt}$ from boundary is restricted, while VCF of bulk spins can be approximated by a delta function $\delta(t)$.

The Fourier transforms of the VCF tensor $D(\omega) = \int_0^\infty \langle v(t)v(0)\rangle_c e^{i\omega t}\, dt$ and spin dephasing, $\mathbf{F}(\omega,\tau) = \int_0^\tau \mathbf{F}(t)e^{i\omega t}\, dt$, convert Eq. (4) in a more compact form [13], which is for the isotropic diffusion [11]

$$\beta(\mathbf{r},\tau) = \frac{1}{\pi}\int_0^\infty |\mathbf{F}(\mathbf{r},\omega,\tau)|^2 D(\mathbf{r},\omega)\, d\omega. \tag{8}$$

The signal attenuation depends on the spectra of the spin dephasing. The power spectrum of the sum of applied (index a) and internal (index s) gradients is

$$|\mathbf{F}(\mathbf{r},\omega,\tau)|^2 = |\mathbf{F}_a(\omega,\tau)|^2 + 2\,\mathrm{Re}\,[\mathbf{F}_a(\omega,\tau)\cdot\mathbf{F}_s^*(\mathbf{r},\omega,\tau)] + |\mathbf{F}_s(\mathbf{r},\omega,\tau)|^2. \tag{9}$$

We can shift the spectrum peak of the susceptibility dephasing F_s away from the spectrum peak of the applied gradient F_a with an adequate combination of RF and applied gradient pulses and therefore diminish the influence of the mixed term on the echo attenuation. If $\mathbf{G}_a \gg \mathbf{G}_s(\mathbf{r})$ the mixed term $\mathrm{Re}[F_a(\omega)F_s^*(\omega)]$ is much larger then $|F_s(\omega)|^2$ and represents the dominant effect of susceptibility. For instance, spectra $F_a(\omega)$ and $F_s(\omega)$ of a PGSE sequence applied in a steady internal susceptibility gradient (Fig. 1A)

$$\mathbf{F}_a = \frac{4\gamma\mathbf{G}_a \sin\frac{\omega\delta}{2}\sin\frac{\omega\Delta}{2} e^{i\omega\delta/2}e^{i\omega\Delta/2}}{\omega^2} \tag{10}$$

and

$$\mathbf{F}_s = \frac{4\gamma\mathbf{G}_s \sin^2\frac{\omega\tau}{4} e^{i\omega\tau/2}}{\omega^2} \tag{11}$$

are shown in Fig. 1B.

Both spectra have a distinct peak at the zero frequency, while in the CPMG RF pulse train interspersed with the pulsed gradient sequence (Fig. 2A), the peaks of $F_s(\omega)$ and $F_a(\omega)$ overlap only partially (Fig. 2B). The $F_a(\omega)$ term is the same as in the PGSE sequence, but the peak of the $F_s(\omega)$ spectra is shifted toward the frequency, defined by the delay between the successive π pulses, and is given by

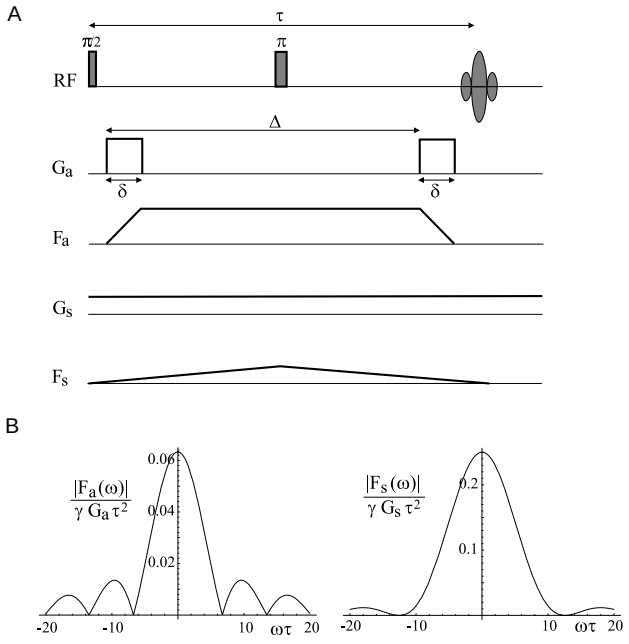

Fig. 1. (A) The combination of RF and applied gradient pulses G_a in a PGSE experiment; δ is the length of the gradient pulse, Δ is the time between two successive gradient pulses. The spin echo is formed at a time τ after the $\pi/2$ pulse. The internal magnetic field gradient G_s is time-independent. Corresponding factors of spin dephasing are denoted by F_a and F_s. (B) Frequency spectra of spin dephasing factors have distinct peaks at the zero frequency. The width of the peak is defined with $1/\Delta$ for $F_a(\omega)$ and $1/\tau$ for $F_s(\omega)$.

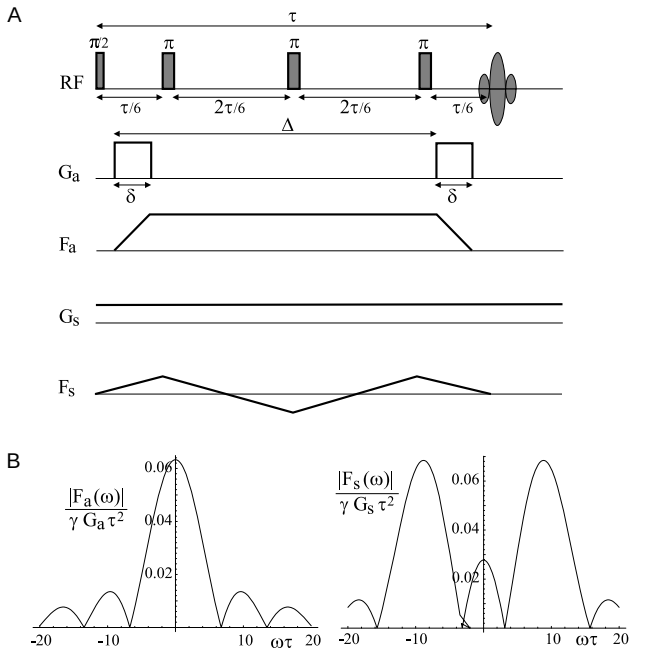

Fig. 2. (A) The CPMG RF pulse train interspersed with a pulsed field gradient sequence; δ is the length of the gradient pulse, Δ is the time between the two successive gradient pulses. The spin echo is formed at a time τ after the $\pi/2$ pulse. The internal magnetic field gradient G_s is time-independent. π pulses follow the excitation $\pi/2$ pulse at times $\tau/6$, $\tau/2$, and $5\tau/6$. The corresponding factors of spin dephasing are denoted by F_a and F_s. (B) The frequency spectra of spin dephasing factors. The spectrum of the applied gradient dephasing is identical to the one in Fig. 1. The zero-frequency peak of the internal spin dephasing factor is shifted to a higher frequency $3\pi/\tau$. The peaks of the spectra do not overlap which significantly reduce the effect of susceptibility gradient.

$$\mathbf{F}_s = \frac{4\gamma \mathbf{G}_s \sin^2 \frac{\omega\tau}{12} (2\cos\frac{\omega\tau}{3-1}) e^{i\omega\tau/2}}{\omega^2}. \quad (12)$$

The mixed term $(2\mathrm{Re}[F_a(\omega)F_s^*(\omega)])$ of the PGSE sequence is substantially higher then the same term of a CPMG sequence, as can be seen in Fig. 3. Hence, results

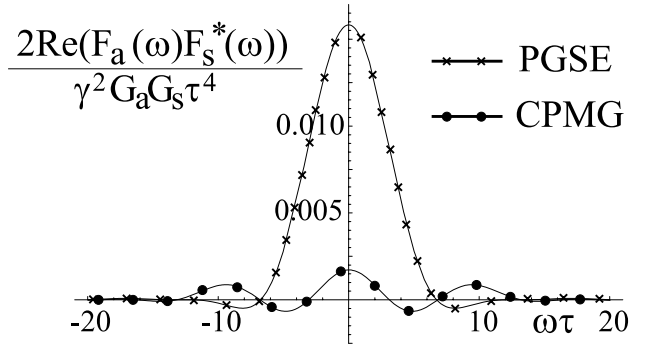

Fig. 3. Mixed terms of Eq. (9) for PGSE and CPMG sequences in a steady susceptibility gradient. The CPMG term is substantially lower (approx. 9 times lower than PGSE term) because the peak of the susceptibility gradient dephasing spectrum $F_s(\omega)$ does not overlap with the peak of the applied gradient dephasing spectrum $F_a(\omega)$.

of measurements by the CPMG sequence are far less influenced by the susceptibility gradient. In addition to that, the mixed term can have a negative sign, if the applied gradient and the susceptibility gradient oppose each other, and the diffusion-weighted signal can actually be stronger in the proximity of boundaries.

2. Results and discussion

The method of reducing the susceptibility effect by applying extra π pulses is demonstrated by a series of diffusion-weighted images of water contained in a narrow notch milled in a cylindrical piece of Plexiglas that has large susceptibility as shown in Table 1. The width of 10 mm long and 9 mm deep notch was 2.8 mm, while the diameter of the Plexiglas cylinder was 10 mm. The experiment was carried out using a TecMag NMR spectrometer with a horizontal bore 2.35-T superconductive magnet equipped with microimaging accessories. The gradient system can produce magnetic field gradient up to 400 mT/m at the slew rate 3000 (mT/m)/ms. After the notch was filled with distilled water the sample was inserted horizontally with the notch walls being vertical into a 10 mm saddle-shaped RF coil. The notch was carefully aligned with respect to the direction of the applied gradient $\mathbf{G}_a$ and the static magnetic field $\mathbf{B}_0$; the notch walls were normal to the applied gradient direction and were with their long side parallel to the static magnetic field (Fig. 4). 1D signal intensity profiles in the normal direction to the walls were measured by the sequences of two gradient pulses: the compensation and the readout gradient with a different number and order of π RF pulses in between is used. To improve the signal-to-noise ratio, each 1D profile was obtained as an average of 50 signal acquisitions with the 3 s recovery time. The imaging field of view was 20 mm, which yields at a 50 kHz acquisition frequency bandwidth the readout gradient of strength 120 mT/m. As the signal was acquired in 1024 points, the image resolution was 20 μm per pixel and the signal readout time was 10.24 ms. Readout gradient was slightly longer due to a 1 ms long crusher/stabilization gradient applied before the signal acquisition. Another 6.12 ms long gradient of the same polarity and strength was applied immediately after the excitation pulse and before the π pulses to compensate the first half of the readout gradient and hence align the center of the acquisition with the k-space center. Both

Table 1
Susceptibility

Substance	χ (10^{-6})
Water	−0.72
SiO_2	−1.14
Plexiglas	−3.24

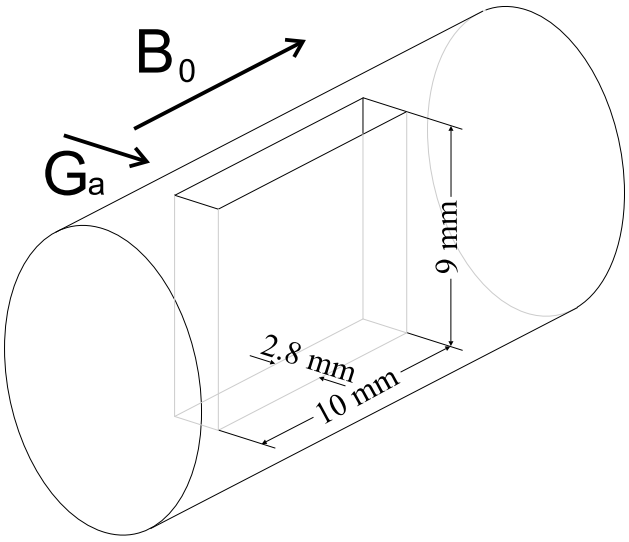

Fig. 4. The sketch of the sample geometry. A narrow notch was milled in a cylindrical piece of Plexiglas that has large susceptibility and carefully filled with water. The width of 10 mm long and 9 mm deep notch is 2.8 mm, while the diameter of the Plexiglas cylinder is 10 mm. The notch was carefully aligned with respect to the direction of the applied gradient $\mathbf{G}_a$ and the static magnetic field $\mathbf{B}_0$; the notch walls were normal to the applied gradient direction and were with their long side parallel to the static magnetic field.

gradients, the readout gradient and the compensation gradient, were also used for signal diffusion weighting. All pulses used in the sequence were hard; the duration of the excitation $\pi/2$ pulse was 4 μs, while the π pulse was 8 μs long.

Fig. 5 shows images, taken with a sequence of two gradient pulses with a single π pulse in between (Fig. 1A), for two different values of $\Delta = 84$ ms and $\Delta = 114$ ms. In both cases the narrow peaks near the boundaries indicate the effect of the diffusive edge enhancement. The edge enhancement is accompanied with a distortion that extends along the width of the notch. The images in Fig. 6 are the result of the CPMG sequence from Fig. 2. The images were acquired at the same intergradient delay Δ and the same gradient strength as images in Fig. 5. The images correspond to the images predicted by the theory and computer simulation in the case of $G_s = 0$ [14]. For the comparison, the difference between PGSE and CPMG measurements is plotted in Fig. 7. The plot of signal difference suggests what is the internal magnetic field induced by the susceptibility difference. The observed spatial variation of the internal magnetic field is the result of the finite notch size and therefore becomes significant near the bound-

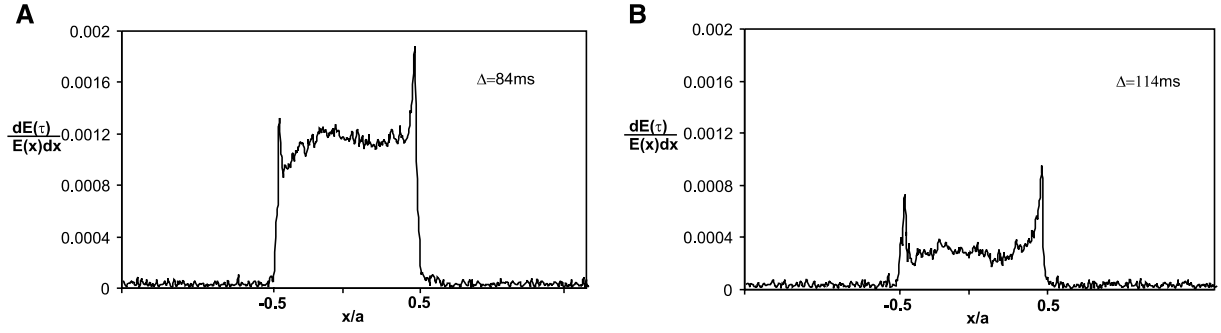

Fig. 5. The diffusion-weighted 1D MR micro images obtained by the PGSE in which the second gradient pulse was prolonged to acquire the signal. The edge enhancement is accompanied with a distortion that extends along the width of the notch because internal magnetic field reduces the effect of the external magnetic field gradient. The imaging parameters were $D = 2 \times 10^{-9}$ m^2/s, $G_a = 120$ mT/m, $\delta = 6.12$ ms, $\Delta = 84$ ms for image A and $\Delta = 114$ ms for image B.

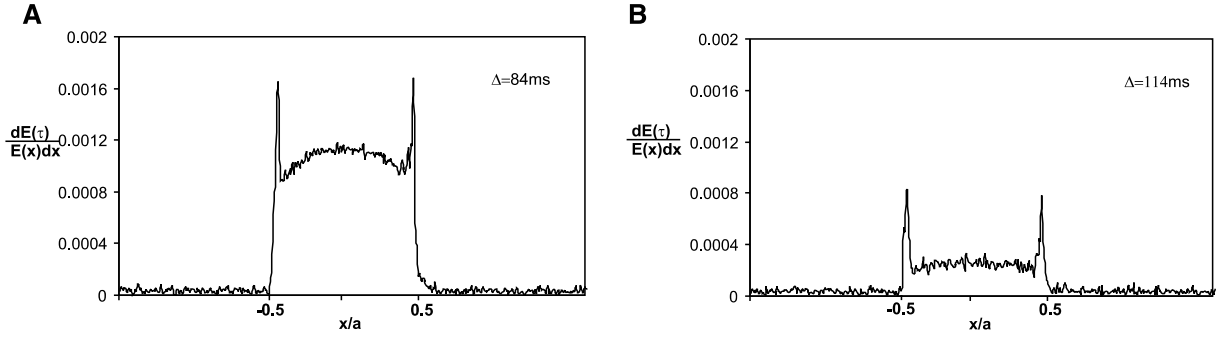

Fig. 6. The diffusion-weighted 1D MR micro images obtained by the modified PGSE with a CPMG RF pulse train designed to reduce susceptibility effects. The second gradient pulse was prolonged to acquire the signal. The signal in the centre of the profile is attenuated as expected for the free self-diffusion, while the edges are enhanced because molecular motion in proximity of impermeable walls is restricted. The imaging parameters were $D = 2 \times 10^{-9}$ m^2/s, $G_a = 120$ mT/m, $\delta = 6.12$ ms, $\Delta = 84$ ms for image A and $\Delta = 114$ ms for image B.

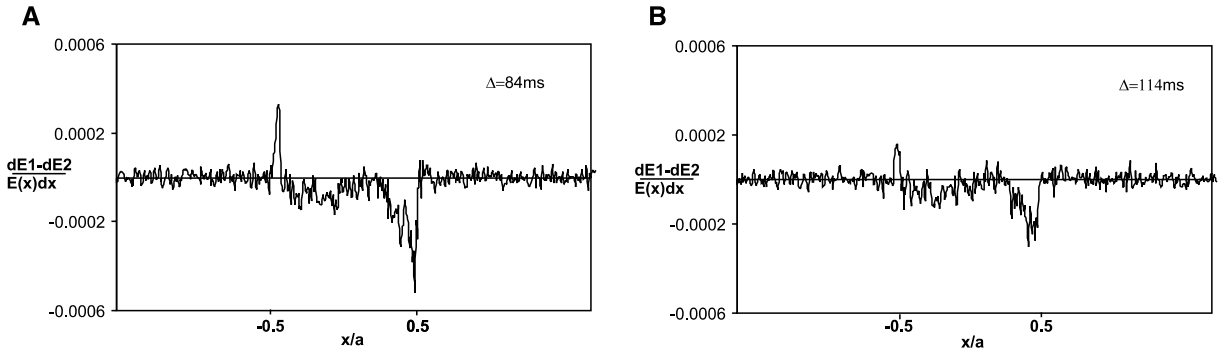

Fig. 7. The difference between diffusion-weighted 1D MR micro images obtained by the CPMG measurement (E_1) and PGSE measurement (E_2). It suggests what is the internal magnetic field induced by the susceptibility difference. The observed spatial variation of the internal magnetic field is the result of the finite notch width and therefore becomes significant near the boundaries. The imaging parameters were the same as for Figs. 5 and 6.

aries. The order of magnitude of the internal magnetic field gradient can be estimated [8] from

$$G_s \approx \frac{(\chi_w - \chi_p)B_0}{d} = 2.2\,\mathrm{mT/m}, \tag{13}$$

where χ_p is the susceptibility of Plexiglas, χ_w is the susceptibility of water, B_0 is 2.35 T, and d is the width of the notch (2.8 mm). Better estimation can be obtained from the plot of the signal difference (Fig. 7). The difference between diffusion-weighted 1D MR micro images acquired by the CPMG sequence (E_1) and the PGSE sequence (E_2) can be approximated by

$$\begin{aligned}\Delta E &= E_1 - E_2 \\ &\approx E_0 e^{-\gamma^2 G_a^2 \delta^2 D\Delta}\left(e^{-\gamma^2 G_a G_s \delta D\Delta^2/18} - e^{-\gamma^2 G_a G_s \delta D\Delta^2/2}\right) \\ &\approx E_1 \frac{4}{9}\gamma^2 G_a G_s D\delta\Delta^2,\end{aligned} \tag{14}$$

where $G_a \gg G_s$ is assumed. Note that according to Fig. 3 the CPMG mixed term can have different sign than the PGSE mixed term. From Eq. (14) the following approximation of the internal magnetic field magnitude can be derived

$$G_s \approx \frac{\Delta E}{E_1}\frac{9}{4\gamma^2 G_a D\delta\Delta^2} = 0.8\,\mathrm{mT/m}. \tag{15}$$

3. Conclusion

The spectral analysis of spin echo enables to resolve, in a simple way, how various RF-gradient pulse sequences reduce the effect of the internal magnetic field induced by the susceptibility difference at interfaces. The method helps in designing a proper RF-gradient pulse sequence. The proper sequence amplifies effects of applied gradient and reduces the spin echo attenuation due to the magnetic susceptibility differences. The method is demonstrated by the 1D diffusion-weighted MR imaging of water in the narrow notch milled in piece of Plexiglas. The method is useful to distinguish the susceptibility effect from the effects of applied gradients when investigating the transport of fluid through a porous structure.

Acknowledgments

We are grateful to the Slovenian Ministry of Education, Science and Sport for the financial support.

References

[1] B.W. Hyslop, P.C. Lauterbur, J. Magn. Reson. 94 (1991) 501–510.
[2] T.M. de Swiet, P.N. Sen, J. Chem. Phys. 100 (1994) 5597–5604.
[3] P.T. Callaghan, A. Coy, L.C. Forde, C.J. Rofe, J. Magn. Reson. A 101 (1993) 347–350.
[4] W.D. Williams, E.F.W. Seymour, R.M. Cotts, J. Magn. Reson. 31 (1978) 271–282.
[5] R.F. Karlicek, I.J. Lowe, J. Magn. Reson. 37 (1980) 75–91.
[6] P. Kinchesh, E.W. Randall, K. Zick, J. Magn. Reson. 100 (1992) 411–415.
[7] D. van Dusschoten, P.A. de Jager, H. Van As, J. Magn. Reson. A 112 (1995) 237–240.
[8] P.T. Callaghan, Principles of Nuclear Magnetic Resonance Microscopy, Oxford University Press, Oxford, 1991.
[9] J. Kärger, W. Heink, J. Magn. Reson. 51 (1983) 1–7.
[10] D.G. Cory, A.N. Garroway, Magn. Reson. Med. 4 (1990) 435–444.
[11] J. Stepišnik, Physica B 104 (1981) 350–364.
[12] P.T. Callaghan, A. Coy, D. MacGowan, K.J. Packer, F.O. Zelaya, Nature 351 (1991) 467–469.
[13] J. Stepišnik, Physica B 270 (1999) 110–117.
[14] A. Duh, A. Mohorič, J. Stepišnik, J. Magn. Reson. 148 (2001) 257–266.